

Performance Analysis of One-Bit Massive MIMO with Superimposed Pilots

M.A. Teeti, *Member, IEEE*, Rui Wang, *Member, IEEE*, and Reza Abdoolee, *Member, IEEE*,

Abstract—In this work, we consider a 1-bit quantized Massive MIMO channel with superimposed pilots (SP), dubbed “QSP”. With linear minimum mean square error (LMMSE) channel estimator and maximum ratio combining (MRC) receiver at the BS, we derive an approximate lower bound on the ergodic achievable rate. When optimizing pilot and data powers, the optimal power allocation maximizing the data rate is obtained in a closed-form solution. We demonstrate that quantization noise is not critical and the data rate converges to a deterministic value as the number of BS antennas grows without limit. When considering a 1-bit quantized Massive MIMO channel with multiplexed-pilots (QTP), it is shown that QSP can outperform the non-optimized QTP in many cases. Moreover, we demonstrate that the gap between QSP, with and without pilot removal after estimating the channel, is not significant. Numerical results are presented to verify our analytical findings and insights are provided for further research on SP.

Index Terms—Massive MIMO, superimposed pilots, time-multiplexed pilots, 1-bit ADC.

I. INTRODUCTION

Equipping the base-station (BS) in large-scale multiple-input multiple-output (MIMO) system (aka Massive MIMO) with low-resolution ADCs (analogue-to-digital converters) or DACs (digital-to-analogue converters) has become a popular research in recent years. The main advantage of using low-resolution ADCs/DACs is that it provides a potential for a great reduction in the expensive hardware components, amount of baseband data to be processed and power consumption at the base station (BS). This is a very valuable feature for Massive MIMO, especially when the number of BS antennas grows large or/and larger bandwidths are used, such as in mmWave bands. For instance, consumed power per single ADC scales exponentially with the number of quantization bits [1] [2] and the generated baseband data at the BS—if, say, 12-bit resolution ADCs/DACs are used—is enormous, that cannot be supported by any existing technologies.

A. Related works

The adoption of low-resolution ADCs/DACs (say, 1-3 bits) has become a focal research area recently [3] [4] [5]. Due to its extreme simplicity, there has been a surge of interest in the 1-bit resolution ADC, where each antenna is attached to a pair of ADCs, each per signal dimension. Interestingly, 1-bit

ADC is reduced to an on-off switch, thereby the need for an automatic gain control unit is unnecessary. As a byproduct for this appealing solution, a magnificent reduction in hardware complexity and power consumption can be achieved [6].

In quantized systems, the received signal impinged at the BS undergoes nonlinear distortion. In particular, this distortion becomes very severe when 1-bit ADCs are employed since the original baseband signal is now replaced by its polarity (per signal dimension) with respect to (w.r.t.) a predetermined threshold. As a result, the channel estimation at the BS becomes challenging [7], which will, in turn, impact the performance. This is of great importance in Massive MIMO as enabling its promising high spectral efficiency hinges on the accuracy of channel state information (CSI) available at the BS [8].

In [3], the 1-bit quantized Massive MIMO with QPSK signaling is considered. Although such very coarse quantization is used, it was shown that high data rates can be still achieved when LS (least-squares) channel estimator, and maximum ratio combining (MRC) or zero-forcing (ZF) receiver are used. In [9], the authors study the uplink in a wideband Massive MIMO channel where 1-bit ADCs are considered. With the assumption on quantization noise (QN) being independent and identically distributed (IID), LMMSE (linear minimum mean square error) channel estimator and MRC/ZF receivers, a lower bound on the ergodic achievable rate is established. Moreover, it is shown that the IID assumption on QN becomes increasingly accurate as the number of users or number of channel taps is sufficiently large and hence the loss of information resulting from that assumption is negligible.

In [10], a more accurate model which captures the temporal/spatial correlation of QN is considered, assuming a 1-bit quantized single-cell Massive MIMO. Given that the quantizer’s input is Gaussian, the authors in [10] use the Bussgang theorem [11] to decompose the quantizer’s output into two parts; the unquantized signal plus a generally correlated QN, while the QN itself is uncorrelated to the signal. Compared with the case when QN is assumed to be IID, it is shown that taking into account correlation among QN samples can further improve channel estimate, especially when input signal is correlated. Moreover, when channel fading follows Rayleigh distribution, it turns out that the IID assumption on QN serves as a good approximation when operating in low signal-to-ratio (SNR) regimes or the number of users is sufficiently large, validating the observations found in [9]. Based on the capacity lower-bounds derived in [10] for MRC and ZF receivers, it was concluded that high spectral efficiencies can be achieved in single-cell scenarios.

M. Teeti and R. Wang are with the Department of Electrical and Electronic Engineering, Southern University of Science & Technology of China, Shenzhen, 518055, China (e-mail:moha@sustc.edu.cn, wang.r@sustc.edu).

R. Abdoolee is with the Department of Computer & Electrical and Computer Science, California State University, Bakersfield, 93311 California (email: rabdoolee@csu.edu).

In [4], the authors generalize the 1-bit quantized model in [10] to an arbitrary number of quantization bits. Therefore, they show that high-order modulation is possible even under 1-bit quantized case, whereas with a few bits, one can approach the rate achieved when infinite-resolution ADCs are used. In contrast to unquantized channels, it has long been known that the structure of pilot sequences has a great impact on the performance [7]. More recently, it has been shown in [9] that, given a fixed average power, pilot sequences with dense representation in time domain are preferable over sparse pilot sequences.

In previous works on the 1-bit quantized Massive MIMO have focused on *time-multiplexed pilots* (TP) [12] [13], where pilot and data symbols are orthogonal in time domain. In TP approach, pure pilot sequences of length, say τ symbols, are sent by all users at the start of transmission for the purpose of channel estimation at the BS. Then, data communication takes place afterwards over $T - \tau$ symbol intervals, where T is the coherence time of the channel over which the channel is assumed constant. An interesting and well-known technique called *superimposed pilot* (SP) [14] [15] [16], sends pilot and data symbols side-by-side. This approach is different from TP approach where no data is transmitted during the training phase, thus reduction in spectral efficiency might be incurred under TP. For the *unquantized* Massive MIMO channel, it was shown in [17] that SP has a potential to achieve higher spectral efficiency than TP, especially when advanced signal processing is employed at the BS. More recently, the authors in [18] consider unquantized multicell Massive MIMO channel and derive a rigorous closed-form expression for the ergodic achievable rate in uplink when SP is used. There, it is shown that when both SP and TP approaches are optimized, comparable data rates can be obtained under practical scenarios. This is because pilot contamination resulting in TP can be, in some sense, as bad as data interference in SP due to concurrent transmission of pilots and data. Nevertheless, with more advanced signal processing, it is believed that SP has the potential to outperform TP scheme.

B. Our contributions

In this work, we consider a 1-bit quantized Massive MIMO channel where—in contrast to previous works which assume TP approach—we consider SP approach. Throughout this manuscript we shall refer to the SP approach with 1-bit quantization as *quantized SP* (QSP) and its unquantized (i.e., with infinite-resolution) counterpart as *unquantized SP* (UQSP). A straightforward extension of the work in [18] to quantized MIMO channel is not possible due to the fact that QN (which is not independent of signal) enters in many places in the analysis, rendering the analysis intractable. Nevertheless, utilizing some properties of QN with the aid of some asymptotic results, we derive a closed-form expression for the achievable rate under a block-flat Rayleigh fading while LMMSE channel estimator and MRC receiver are assumed. Due to the lack of explicit formula of the achievable rate under the quantized Massive multicell MIMO channel with TP, we compare QSP against UQSP, whereas the achievable rate

under 1-bit quantization with TP, dubbed “QTP”, is obtained by simulation.

We begin our work by considering a single-cell scenario, then the multicell case is treated afterwards. Most analysis developed under the single-cell case is leveraged for the analysis of performance under the multicell case. Our theoretical findings agree with numerical results to confirm that regardless of the very coarse quantization, SP provides high data rate, and possibly higher than that achieved under TP approach (non-optimized), where more accurate evaluation of QSP against the optimized QTP is left for future work. The main contributions of our work are summarized as follows:

- A closed-form solution for LMMSE channel estimate and its mean-square error are derived for QSP under single-cell and multicell cases. Similar solutions for UQSP and QTP can be recovered as special cases.
- A closed-form expression for the ergodic achievable rate is established, which serves as a good approximation for the achievable rate for QSP. The result is specialized for obtaining a true lower bound on achievable rate under UQSP.
- It is shown that, regardless the coarse quantization and data being submerged in pilots, it is still possible to achieve high data rates in multicell Massive MIMO. It is also shown that QSP can outperform QTP in many cases when QTP is not optimized.
- We show that under 1-bit quantization, pilot removal (PR) after estimating the channel incurs a negligible loss in information under low-SNR regime or large number of users.
- We also show that QN can be averaged out asymptotically with the increase of BS antennas.
- It is demonstrated that under multicell case, for asymptotically large number of BS antennas, the gap between QSP and UQSP vanishes, as the data rates for both cases saturate and converge to a fixed value, given by $\log(1 + \rho_t T / \zeta)$, where T is the coherence time of channel (in symbol intervals), ρ_t is pilot power and ζ is a constant which depends on number of users and geometry of the network.

The rest of the paper is organized as follows. In Sec. II the signal model for the 1-bit quantized single-cell MIMO with SP is presented. In Sec. III equivalent linear model for the quantizer’s output and details of channel estimation are presented. In Sec. IV we derive closed-form expression for the achievable rates under QSP and UQSP when MRC receiver is assumed. In Sec. V, we extend the previous results of achievable rates for a multicell scenario with a special setting. Also, some useful asymptotic results are presented. In Sec. VI, numerical examples for a practical multicell scenario is demonstrated to validate the analytical results and Sec. VII summarizes this paper.

II. SYSTEM MODEL FOR SINGLE-CELL CASE

In the first part of this work, we consider the uplink of a single-cell Massive MIMO. The BS is equipped with M antennas and serves K single-antenna users in the same time-frequency resource. The channel is flat fading which remains

constant over T symbol intervals, i.e., coherence time of the channel. The channel gain between the m -th BS antenna and user k is represented by $\sqrt{\beta_k}h_{mk}$, where β_k and h_{mk} are the large-scale and small-scale fading coefficients, respectively. The coefficients $h_{mk} \sim \mathcal{CN}(0, 1)$ are assumed IID circularly-symmetric complex Gaussian (CSCG) random variables, each with zero-mean and unit-variance. It is assumed that the distance from each user to BS is large enough so that large-scale fading is the same for all antennas.

Each BS antenna is equipped with a pair of 1-bit ADCs for both in-phase and quadrature components of the received signal. The superposition transmission scheme is considered such that the pilot and data symbols are sent simultaneously. For simplicity of analysis, we assume that pilot and data symbols have the same length, T . Thus, over one coherence interval, the BS collects $2MT$ quantized samples (i.e., binary in our case). We assume the BS first estimates the channel using LMMSE, then utilizes the channel estimate for data estimation using MRC receiver. For pilots, we consider all K users use mutually orthogonal sequences. Without loss of generality, we assume pilot sequences are drawn randomly from a Fourier basis matrix. We recall here that such pilot sequences are dense in time domain, thus satisfying the observation in [9] about the preferable pilots being dense in time domain.

Let $\mathbf{x}_k = (x_k[1], x_k[2], \dots, x_k[T])^T$ be a vector of T symbols sent by user k during one coherence interval satisfying power constraint:

$$\frac{1}{T} \mathbb{E} \left\{ \|x_k\|^2 \right\} \leq 1. \quad (1)$$

Further, let $c_k[t]$ and $s_k[t]$ be the pilot and data symbols associated with user k during time instant t , respectively. Then $x_k[t]$ is written as the superposition of $c_k[t]$ and $s_k[t]$:

$$x_k[t] = \sqrt{\alpha_k}c_k[t] + \sqrt{\bar{\alpha}_k}s_k[t], \quad (2)$$

where α_k and $\bar{\alpha}_k$ are the power fractions allocated to pilot and data symbols, respectively, such that $\alpha_k + \bar{\alpha}_k = 1$. Moreover, we assume $\mathbb{E}\{|s_k[t]|^2\} = 1$ and $\sum_{t=1}^T |c_k[t]|^2 = T$, i.e., (1) is satisfied.

In multiuser communication, power control is essential for preventing stronger users from overwhelming weaker users, and hence maintaining some fairness of service. The discrepancy of received powers from different users becomes a critical issue in the 1-bit quantized channels due to saturation effect of ADC when the signal strength exceeds the dynamic range of ADC. Thus power control based on statistical channel-inverse is assumed, similar to the works [10] [18]. The average power of user k , denoted by ρ_k , is

$$\rho_k = \rho/\beta_k, \quad (3)$$

where ρ is a fixed average power, leading to $\alpha_k = \alpha$ and $\bar{\alpha}_k = \bar{\alpha}$, $k \in \{1, 2, \dots, K\}$.

Based on the above discussion, the received complex-baseband signal (unquantized) at the m -th antenna is:

$$y_m[t] = \sum_{k=1}^K \sqrt{\alpha\rho}h_{mk}c_k[t] + \sum_{k=1}^K \sqrt{\bar{\alpha}\rho}h_{mk}s_k[t] + w_m[t], \quad (4)$$

where $w_m[t] \sim \mathcal{CN}(0, 1)$ is the white Gaussian noise which is assumed IID across space and time. The 1-bit quantized signal of (4) with zero-threshold ADCs is:

$$r_m[t] = \frac{1}{\sqrt{2}}\text{sign}(\Re\{y_m[t]\}) + \frac{j}{\sqrt{2}}\text{sign}(\Im\{y_m[t]\}), \quad (5)$$

where $\Re\{\cdot\}$ and $\Im\{\cdot\}$ denote the real and complex parts of a complex quantity, respectively, and $\text{sign}(\cdot)$ is the signum function which returns 1 or -1 when its argument is greater or less than a threshold value, respectively. Thus $r_m[t] \in \mathcal{A} \triangleq \{1 \pm j, -1 \pm j\}$.

Equation (4) can be written in a compact matrix form. Let $\mathbf{s}_k = (s_k[1], \dots, s_k[T])^T$, $\mathbf{c}_k = (c_k[1], \dots, c_k[T])^T$, $\mathbf{h}_k = (h_{1k}, \dots, h_{Mk})^T$, $\mathbf{y}[t] = (y_1[t], \dots, y_M[t])^T$ and $\mathbf{w}[t] = (w_1[t], \dots, w_M[t])^T$ be the length- T vectors of data and pilot symbols, channel vector between user k and all BS antennas, the received signal and white Gaussian noise during time t at all BS antennas, respectively. Moreover, we let $\mathbf{r}[t] = (r_1[t], \dots, r_M[t])^T$ and $\mathbf{z}[t] = (z_1[t], \dots, z_M[t])^T$ be the vectors of quantized signal and QN, during time t at all BS antennas. Rearranging (4) for all $m = 1, 2, \dots, M$ and $t = 1, 2, \dots, T$, the $M \times T$ received signal can be written as

$$\mathbf{Y} = \sqrt{\alpha\rho}\mathbf{H}\mathbf{C} + \sqrt{\bar{\alpha}\rho}\mathbf{H}\mathbf{S} + \mathbf{W}, \quad (6)$$

and hence the corresponding quantized signal is

$$\mathbf{R} = \frac{1}{\sqrt{2}}\text{sign}(\Re\{\mathbf{Y}\}) + \frac{j}{\sqrt{2}}\text{sign}(\Im\{\mathbf{Y}\}), \quad (7)$$

where $\mathbf{Y} = (\mathbf{y}[1], \dots, \mathbf{y}[T])$, $\mathbf{R} = (\mathbf{r}[1], \dots, \mathbf{r}[T])$, $\mathbf{W} = (\mathbf{w}[1], \dots, \mathbf{w}[T])$ is a $M \times T$ white Gaussian noise matrix, and \mathbf{H} , \mathbf{C} and \mathbf{S} are the composite channel, pilot and data matrices, defined as $\mathbf{H} = (\mathbf{h}_1, \dots, \mathbf{h}_K) \in \mathbb{C}^{M \times K}$, $\mathbf{C} = (\mathbf{c}_1, \dots, \mathbf{c}_K) \in \mathbb{C}^{K \times T}$ and $\mathbf{S} = (\mathbf{s}_1, \dots, \mathbf{s}_K) \in \mathbb{C}^{K \times T}$.

III. LINEAR MODEL AND CHANNEL ESTIMATION

The model equation (5) is nonlinear, rendering analytical evaluation of system performance intricate. However, if quantizer's input is Gaussian, the Bussgange decomposition [11] can be used to decompose the quantizer's output into a sum of scaled version of its input and uncorrelated QN, where the QN itself is temporally or/and spatially correlated, [9]. Unfortunately, Bussgange's decomposition involves another nonlinear operation, namely, the *arcsin law* which makes the analysis intractable, i.e., see [19] [10] for more details. Nevertheless, Bussgange decomposition is used in this work to simplify analysis, then we impose the IID assumption on QN to obtain closed-form formulae for the channel estimator and achievable rates, where this assumption turns out to be a good approximation in Massive MIMO scenarios as will be demonstrated by numerical results.

A. Assumptions

In order to proceed with the development of theoretical results, we allow the following assumptions:

- 1) All data symbols $\{s_k[t]\}$ are assumed to be IID CSCG random variables. This has been a standard assumption in

the literature which allows to use existing lower-bounding techniques to obtain a lower bound on capacity.

- 2) The unquantized signals $\{y_m[t]\}$ are assumed to be Gaussian random variables. This assumption can be easily justified by the central limit theorem (CLT) as the distribution of $y_m[t]$ tends towards Gaussian with zero-mean and variance $\sigma_y^2 = K\rho + 1$, for asymptotically large K . For K being sufficiently large should come at no surprise in Massive MIMO, especially when considering multicell scenario where total number of users is KL where L is the number of cells. Therefore, this assumption is reasonable.
- 3) At low-SNR regime or large K , the QN is approximately IID [9] [10].

B. Equivalent channel model and its statistical properties

Let $\bar{\mathbf{y}}_m, \bar{\mathbf{r}}_m, \bar{\mathbf{z}}_m$ and $\bar{\mathbf{w}}_m$ be the column vectors constructed from the m -th rows of $\mathbf{Y}, \mathbf{R}, \mathbf{Z}$ and \mathbf{W} , respectively. Further, we define $\bar{\mathbf{h}}_m$ as the column vector of the channel from all K users to m -th BS antenna. We use bars over all symbols to distinguish them from the original columns of corresponding matrices. Under Rayleigh fading, the rows of \mathbf{Y} are IID with a common covariance matrix $\Sigma_{\bar{\mathbf{y}}_m} \triangleq \mathbb{E}\{\bar{\mathbf{y}}_m \bar{\mathbf{y}}_m^H\}$, given by

$$\Sigma_{\bar{\mathbf{y}}_m} = \alpha\rho\mathbf{C}\mathbf{C}^H + (\bar{\alpha}K\rho + 1)\mathbf{I}_T, \quad m \in \{1, \dots, M\}. \quad (8)$$

Therefore, without loss of generality, we will only focus on the analysis based on $\bar{\mathbf{y}}_m$.

By Busgang's decomposition, $\bar{\mathbf{r}}_m$ can be written as $\bar{\mathbf{r}}_m = \mathbf{B}\bar{\mathbf{y}}_m + \bar{\mathbf{z}}_m$, where \mathbf{B} is a linear operator which is chosen such that $\bar{\mathbf{z}}_i$ is uncorrelated with $\bar{\mathbf{y}}_m$, i.e.,

$$\mathbb{E}\{z_m^*[t]y_m[t']\} = 0, \quad \forall t, t' \in \{1, \dots, T\}. \quad (9)$$

From [10], it is easy to show that \mathbf{B} admits the simple form $\mathbf{B} = \sqrt{\gamma}\mathbf{I}$, where γ is defined as

$$\gamma \triangleq 2/(\pi\sigma_y^2), \quad (10)$$

and hence $\bar{\mathbf{r}}_m$ takes the following form:

$$\bar{\mathbf{r}}_m = \sqrt{\gamma}\bar{\mathbf{y}}_m + \bar{\mathbf{z}}_m. \quad (11)$$

From (11), the covariance matrix of quantization noise, defined as $\Sigma_{\bar{\mathbf{z}}_m} \triangleq \mathbb{E}\{\bar{\mathbf{z}}_m \bar{\mathbf{z}}_m^H\}$, is given by $\Sigma_{\bar{\mathbf{z}}_m} = \Sigma_{\bar{\mathbf{r}}_m} - \gamma\Sigma_{\bar{\mathbf{y}}_m}$, where $\Sigma_{\bar{\mathbf{r}}_m} \triangleq \mathbb{E}\{\bar{\mathbf{r}}_m \bar{\mathbf{r}}_m^H\}$ is the autocorrelation matrix of quantizer's output. It is well-known that when quantizer input is Gaussian, $\Sigma_{\bar{\mathbf{r}}_m}$ follows the arcsin law [20]. However, working with the nonlinear arcsin operator seems to add another level of complexity of analysis. By Assumption 3), the covariance matrix of QN reduces to a diagonal matrix given by [10]:

$$\Sigma_{\bar{\mathbf{z}}_m} \approx \sigma_z^2 \mathbf{I}_T. \quad (12)$$

where $\sigma_z^2 = 1 - 2/\pi$.

Under QTP, it was shown in [9] [10] that QN is not only uncorrelated with the input signal but also uncorrelated with channel. For convenience, we state this important result in the following lemma.

Lemma 1. For any $m, m' \in \{1, \dots, M\}$ and any $t \in \{1, 2, \dots, T\}$, we have

$$\mathbb{E}\{z_m^*[t]h_{m'k}\} = 0, \quad t = 1, \dots, T. \quad (13)$$

Proof. The proof can be found in [9] [10]. ■

Not surprisingly, Lemma 1 is still valid when SP is used. We will use Lemma 1 when deriving the LMMSE channel estimator.

C. LMMSE channel estimation

We use the quantized signal (11) to derive the LMMSE channel estimator for QSP. For UQSP, LMMSE estimator can be recovered as a special case when QN is set to zero. Consider the sufficient statistic u_{mk} given by

$$u_{mk} \triangleq \mathbf{c}_k^H \bar{\mathbf{r}}_m = T\sqrt{\alpha\rho\gamma}h_{mk} + v_{mk}, \quad (14)$$

where v_{mk} is an effective noise (non-Gaussian) given by

$$v_{mk} = \sqrt{\alpha\rho\gamma}\mathbf{c}_k^H \mathbf{S}^T \bar{\mathbf{h}}_m + \sqrt{\gamma}\mathbf{c}_k^H \bar{\mathbf{w}}_m + \mathbf{c}_k^H \bar{\mathbf{z}}_m. \quad (15)$$

The channel estimate and variance of estimation error are given in the following lemma.

Lemma 2. Consider QSP with Assumption 3 holds, the LMMSE estimate of h_{mk} , denoted by \hat{h}_{mk} , is

$$\hat{h}_{mk} = \frac{\sqrt{\alpha\rho\gamma}}{\alpha\rho\gamma T + \bar{\alpha}\rho K\gamma + \gamma + \sigma_z^2} u_{mk} \quad (16)$$

and the variance of estimation error $\tilde{h}_{mk} \triangleq h_{mk} - \hat{h}_{mk}$ is

$$\sigma_{\tilde{h}}^2 = 1 - \frac{\alpha\rho T}{\alpha\rho T + \bar{\alpha}\rho K + 1 + \sigma_z^2/\gamma} \quad (17)$$

Proof. The proof follows from standards LMMSE channel estimate given by $\hat{h}_{mk} = \frac{\mathbb{E}\{h_{mk}u_{mk}^*\}}{\mathbb{E}\{|u_{mk}|^2\}}u_{mk}$ and making use of Lemma 1 when computing $\mathbb{E}\{h_{mk}u_{mk}^*\}$. ■

The channel estimate and its error variance for UQSP can be recovered from Lemma 2. Thus we are led to following lemma:

Lemma 3. For UQSP, the LMMSE estimate of h_{mk} , denoted by \hat{h}_{mk} , is given by

$$\hat{h}_{mk} = \frac{\sqrt{\alpha\rho}}{\alpha T\rho + \bar{\alpha}K\rho + 1} \bar{u}_{mk} \quad (18)$$

and variance of estimation error is

$$\bar{\sigma}_{\tilde{h}}^2 = 1 - \frac{\alpha T\rho}{\alpha T\rho + \bar{\alpha}K\rho + 1}. \quad (19)$$

where $\bar{u}_{mk} = \sqrt{\alpha\rho\gamma}\mathbf{c}_k^H \mathbf{S}^T \bar{\mathbf{h}}_m + \sqrt{\gamma}\mathbf{c}_k^H \bar{\mathbf{w}}_m$.

Proof. Note that under UQSP, $\bar{\mathbf{r}}_m = \bar{\mathbf{y}}_m$ and $\bar{\mathbf{z}}_m = 0$ (or equivalently, $\sigma_z^2 = 0$ and $\gamma = 1$). Thus by redefining (14)- (17) according to this change, (18) and (19) follow immediately. ■

By inspecting Lemmas 2 & 3, it is obvious that the variance of estimation error can be made arbitrarily small by increasing the length of pilot sequences.

It is worth pointing out that the LMMSE channel estimate \hat{h}_{mk} for QSP doesn't coincide with the MMSE solution, thereby \hat{h}_{mk} is not Gaussian distributed. This is because the estimation is based on the discrete-valued observation vector $\bar{\mathbf{r}}_m$ rather than Gaussian observation. Notwithstanding

this, \hat{h}_{mk} can still be approximated as Gaussian. This elicits from the fact that \hat{h}_{mk} is a weighted sum of T random variables (each of cardinality $|\mathcal{A}| = 4$), where in practical cellular systems, T can span tens or a few hundreds of symbol intervals. Thus, by the CLT, the distribution of \hat{h}_{mk} tends to be Gaussian.

Finally, we close this section by making the following remark which will prove useful in the analysis of achievable rates.

Remark 1. It is important to notice that under QSP, the channel estimate \hat{h}_{mk} (and hence its estimation error \tilde{h}_{mk}) is not only dependent on data symbols transmitted from all users, but also on the white Gaussian noise $\tilde{\mathbf{w}}_m$ and the quantization noise $\tilde{\mathbf{z}}_m$. Certainly, this is a highly undesirable property which renders the capacity analysis more complicated as will be seen later.

IV. ANALYSIS OF ACHIEVABLE RATES

In this section we establish an approximation for the lower bound on the ergodic achievable rate for QSP and UQSP when the MRC receiver is employed at the BS. Without loss of generality, we focus on the information rate of the k -th user during an arbitrary time t .

We denote by $\mathbf{r}[t] \in \mathbb{C}^M$ the received quantized signal across all BS antennas during time t , i.e., the t -th column of \mathbf{R} . Let $\bar{\mathbf{s}}[t] = [s_1[t], s_2[t], \dots, s_K[t]]^T$ and $\bar{\mathbf{c}}[t] = [c_1[t], c_2[t], \dots, c_K[t]]^T$ be the column vectors of \mathbf{S} and \mathbf{C} , respectively. Further, we stack all channel estimates $\{\hat{h}_{mk}\}$ of the k -th user as a column vector given by $\mathbf{h}_k = [\hat{h}_{1k}, \dots, \hat{h}_{mk}, \dots, \hat{h}_{Mk}]^T$. Thus we have

$$\hat{\mathbf{h}}_k = \xi \mathbf{R} \mathbf{c}_k^*, \quad (20)$$

where $\xi \triangleq \sqrt{\alpha\rho\gamma}/(\alpha\rho\gamma T + \bar{\alpha}\rho K\gamma + \gamma + \sigma_z^2)$.

Having estimated the channel, the contribution of pilot signals can be removed from $\mathbf{r}[t]$, utilizing the channel estimates $\{\hat{\mathbf{h}}_k\}_{k=1}^K$, as follows:

$$\begin{aligned} \mathbf{r}^{\text{PR}}[t] &\triangleq \mathbf{r}[t] - \sqrt{\alpha\rho\gamma} \hat{\mathbf{H}} \bar{\mathbf{c}}[t] \\ &= \sqrt{\alpha\rho\gamma} \mathbf{H} \bar{\mathbf{s}}[t] + \sqrt{\gamma} \mathbf{w}[t] + \mathbf{z}[t] + \sqrt{\alpha\rho\gamma} \tilde{\mathbf{H}} \bar{\mathbf{c}}[t] \end{aligned} \quad (21)$$

where $\hat{\mathbf{H}} = [\hat{\mathbf{h}}_1 \hat{\mathbf{h}}_2 \dots \hat{\mathbf{h}}_K]$ and $\tilde{\mathbf{H}} = \mathbf{H} - \hat{\mathbf{H}}$ are the composite matrices of channel estimate and estimation error, respectively.

Note that the main challenge of using (21) for capacity analysis stems from the fact that the third term is not independent of the first, second and third terms (see Remark 1). This lends itself to many cross-correlation terms in $\mathbf{r}^{\text{PR}}[t]$ which are difficult to compute in closed-form solutions, making the theoretical analysis intractable. To avoid this intractability and hence obtain a closed-form expression for the achievable rate, PR is not considered in our analysis, similar to the technique used in [18] for analyzing the unquantized MIMO channel with SP. Though PR gives rise to increase in the data rate, it turns out that dispensing PR is not critical as validated by our numerical results.

To proceed, we isolate $s_k[t]$ from the remaining signals in $\mathbf{r}[t]$ as follows:

$$\mathbf{r}[t] = \sqrt{\alpha\rho\gamma} \mathbf{h}_k s_k[t] + \tilde{\mathbf{r}}[t], \quad (22)$$

where $\tilde{\mathbf{r}}[t] \in \mathbb{C}^M$ is a non-Gaussian effective noise given by

$$\begin{aligned} \tilde{\mathbf{r}}[t] &= \sqrt{\alpha\rho\gamma} (\mathbf{H} \bar{\mathbf{s}}[t] - \mathbf{h}_k s_k[t]) + \sqrt{\alpha\rho\gamma} \mathbf{H} \bar{\mathbf{c}}[t] \\ &\quad + \sqrt{\gamma} \mathbf{w}[t] + \mathbf{z}[t], \end{aligned} \quad (23)$$

where the first, second, third and fourth terms are due to data interference from other users (excluding the k -th user), pilot interference of all users, white Gaussian noise and QN, respectively.

Given (22) and the channel estimate $\hat{\mathbf{h}}_k$ in (20), the output of MRC receiver can be written as

$$\hat{s}_k[t] \triangleq \frac{1}{M} \hat{\mathbf{h}}_k^H \mathbf{r}[t] = \frac{\xi}{M} \mathbf{c}_k^T \mathbf{R}^H \mathbf{r}[t], \quad (24)$$

where the scaling factor $1/M$ is introduced here for establishing some asymptotic result later. In the following, a lower bound on the mutual information $I(s_k[t]; \hat{s}_k[t])$ will be derived.

A. Achievable rates for QSP

The exact capacity of (24) is unknown as the distribution of effective noise is not Gaussian, primarily, due to existence of QN. Also, the effective noise might be correlated with the desired signal. The following result holds when the number of BS antennas is sufficiently large, which is the case in Massive MIMO.

Theorem 1. Considering QSP Massive MIMO where QN is assumed to be IID (Assumption 3), if the BS employs LMMSE channel estimation and MRC data estimation, a lower bound on the achievable rate in uplink is approximated by

$$R_{\text{QSP}} = \log(1 + \Upsilon_{\text{QSP}}) \quad (\text{bits/s/Hz}), \quad (25)$$

where Υ_{QSP} is the effective signal-to-noise ratio which is given by (26) at the top of page 13.

Proof. The proof unfolds by representing the output of MRC in (24) as a sum of two parts, desired signal with a multiplicative deterministic channel gain, denoted by a_k , and uncorrelated noise, denoted by $\epsilon_k[t]$, i.e., $\hat{s}_k[t] = a_k s_k[t] + \epsilon_k[t]$. Then the lower bound follows by assuming worst-case (Gaussian) noise with same variance. The details of the proof and hence the closed-form expression for Υ_{QSP} in (26) are shown in Appendix A. ■

The lower bound (25) can be maximized w.r.t. parameter α . The result is stated in the following corollary.

Corollary 4. Let $\alpha^ \in (0, 1)$ be the optimal value of power fraction which maximizes R_{QSP} . Then α^* is given by one of the following two roots:*

$$\alpha^* = \frac{\lambda \pm \sqrt{\lambda \sigma_y^2 (4\rho T(T-K) + (T-1)\sigma_y^2 \pi^2)}}{4\rho(K\rho(T(K+M-T)+1) - T(T-K))} \quad (27)$$

where $\lambda = 4\rho^2 K(MT+1) + \pi^2 \sigma_y^4 (T-1)$.

Proof. By the concavity of $\log(1+x)$ and noticing that the first derivative of R_{QSP} w.r.t. α changes sign due to $R_{\text{QSP}}|_{\alpha=0} = R_{\text{QSP}}|_{\alpha=1} = 0$ (i.e., R_{QSP} is non-monotonic), it follows that α^* can be obtained by solving the quadratic equation $\frac{d}{d\alpha} \Upsilon_{\text{QSP}} = 0$ for α and choosing the positive root that is less than 1. ■

$$\Upsilon_{\text{QSP}} = \left(\bar{\alpha} \alpha \rho^2 T^2 M \right) / \left(\bar{\alpha} \rho^2 K T M + \frac{T}{4} (8 \alpha \bar{\alpha} \rho^2 - 4 \alpha K^2 \rho^2 + \pi^2 K^2 \rho^2 - 4 \alpha K \rho + 2 \pi^2 K \rho + \pi^2) + \alpha^2 K \rho^2 - 2 \alpha K \rho^2 - \frac{1}{4} \pi^2 K^2 \rho^2 + K \rho^2 - \frac{1}{2} \pi^2 K \rho + \alpha \rho T^2 (1 + K \rho) - \frac{\pi^2}{4} \right) \quad (26)$$

B. Achievable rate under UQSP

Deriving the achievable rate for UQSP is straightforward as UQSP is a special case of QSP as mentioned previously, i.e., $\gamma = 1, \sigma_z = 0$ and $\mathbf{r}[t] = \mathbf{y}[t]$. Therefore, we have the following corollary.

Corollary 5. a lowerbound on achievable rate under UQSP system when LMMSE and MRC are used for channel and data estimation, respectively, is

$$R_{\text{UQSP}} = \log(1 + \Upsilon_{\text{UQSP}}) \quad (\text{bits/s/Hz}), \quad (28)$$

where Υ_{UQSP} is given by

$$\Upsilon_{\text{UQSP}} = \left(\alpha \bar{\alpha} \rho^2 T^2 M \right) / \left(\bar{\alpha} \rho^2 K T M + \alpha \rho (K \rho + 1) T^2 + 2 \alpha \bar{\alpha} \rho^2 T + \bar{\alpha} \rho^2 K^2 T + (2 - \alpha) \rho K T + T + \bar{\alpha}^2 \rho^2 K \right) \quad (29)$$

Moreover, the optimal power fraction $\alpha^* \in (0, 1)$ maximizing R_{UQSP} is given by one of the following two roots:

$$\alpha^* = \frac{\delta \pm \sqrt{\delta(T\rho + 1)(K\rho + 1)T}}{\rho(K^2\rho T + K(M\rho T + \rho - \rho T^2 + T) - T^2)} \quad (30)$$

where $\delta = T(K^2\rho^2 + K\rho(M\rho + 2) + 1) + K\rho^2$.

Proof. The proof unfolds by substituting $\gamma = 1, \sigma_z = 0$ and $f(t, t) = (M + 1)\sigma_y^2/M$ in (76) to obtain the normalized variance of effective noise $\tilde{\sigma}_{\epsilon_k}^2$, then substituting $\tilde{\sigma}_{\epsilon_k}^2$ in (64), (28) follows. The second part unfolds straightforwardly by following same lines of the proof of Corollary 4. ■

It is worth pointing out that no approximation techniques are needed in deriving the lower bound (28), in contrast to the lower bound (25).

C. Asymptotic analysis

In (26) and (29) the denominators of Υ_{QSP} and Υ_{UQSP} consists of two main parts: 1) the part (first term) which scales with M and hence we refer to it as the *coherent noise* and 2) the other part (remaining terms) which doesn't scale with M and hence we refer to as *noncoherent noise*. The coherent part for Υ_{QSP} and Υ_{UQSP} is given by $\bar{\alpha} \rho^2 K T M$. As a result, we have the following conclusion on the asymptotic performance comparison between QSP and UQSP.

Corollary 6. The asymptotic limit of data rates for QSP and UQSP when $M \rightarrow \infty$ is

$$R_{\text{QSP}}^{M \rightarrow \infty} = R_{\text{UQSP}}^{M \rightarrow \infty} = \log \left(1 + \frac{\alpha T}{K} \right). \quad (31)$$

Proof. The result follows from taking the limits of both (25) and (28) when $M \rightarrow \infty$, whereas all other parameters are fixed. ■

As can be seen from Corollary 6, both QSP and UQSP are equivalent in the asymptotic sense. In other words, the QN has no effect on performance for asymptotically large number of BS antennas.

V. 1-BIT QUANTIZED MULTICELL MASSIVE MIMO

In this section we extend the previous results of the single-cell case to a multicell case with a network comprised of L cells and K users per cell.

A. Signal model

For simplicity of analysis, we assume that the coherence time of the channel can accommodate KL mutually orthogonal pilot sequences, i.e., no pilot contamination is assumed under SP [17]. We also assume that each K users in each cell employ power control based on statistical channel inverse as in the case of single-cell scenario. In the following, we shall use the same notation as before, while introducing indices of cells. The channel between user k in cell j and the m -th antenna of BS l is defined as $\beta_{ljk} h_{lmjk}$. The pilot and data symbols associated with user k in cell j , sent during time t , are denoted by $c_{jk}[t]$ and $s_{jk}[t]$, respectively. The power assigned to user k in cell j is denoted by ρ_{jk} and its power fractions allocated for pilot and data are denoted by α_{jk} and $\bar{\alpha}_{jk}$, respectively, such that $\alpha_{jk} + \bar{\alpha}_{jk} = 1$.

The received complex-baseband signal at the m th antenna of BS l during time t can be written as

$$y_{lm}[t] = \sum_{j=1}^L \sum_{k=1}^K \sqrt{\eta_{ljk}} h_{lmjk} c_{jk}[t] + \sum_{j=1}^L \sum_{k=1}^K \sqrt{\bar{\eta}_{ljk}} h_{lmjk} s_{jk}[t] + w_{lm}[t], \quad (32)$$

where $\eta_{ljk} = \alpha_{jk} \rho_{jk} \beta_{ljk}$ and $\bar{\eta}_{ljk} = \bar{\alpha}_{jk} \rho_{jk} \beta_{ljk}$. As in the single-cell case, in the multicell case we assume power control based on statistical channel inverse is implemented. Namely, the transmit power of the k -th user in cell j is given by $\rho_{jk} = \beta_{jjk}^{-1} \rho$, where ρ is a fixed power-control coefficient. With this power-control policy, under a Rayleigh-fading model the average power received at each antenna of the j -th BS from each of its K users is the same which is given by ρ .

Let $\theta_{ljk} \triangleq \beta_{ljk} / \beta_{jjk}$ be the ratio between cross (w.r.t. BS l) and direct (w.r.t. to BS j) large-scale coefficients of user k . Consequently, the parameters η_{ljk} and $\bar{\eta}_{ljk}$ in (32) reduce to

$$\eta_{ljk} = \alpha \rho \theta_{ljk}, \quad \text{and} \quad \bar{\eta}_{ljk} = \bar{\alpha} \rho \theta_{ljk}. \quad (33)$$

Since the results are averaged over many realizations (rather than a single realization) of large-scale coefficients, the statistic of $\{\theta_{ljk}\}$ shall be independent of cell index. This is true

due to the random locations of users within each cell which make this assumption reasonable and hence there is no reason to believe they are different for different cell indices (see [21]).

From (32), the variance of $y_{0m}[t]$ is given by

$$\sigma_{y_0}^2 = \kappa_0 \rho + 1, \quad (34)$$

where κ_0 is defined by

$$\kappa_0 \triangleq K + \sum_{j=1, j \neq 0}^L \sum_{k=1}^K \theta_{0jk}. \quad (35)$$

In addition to (35), we also need the following definition:

$$\kappa_1 \triangleq K + \sum_{j=1, j \neq 0}^L \sum_{k=1}^K \theta_{0jk}^2. \quad (36)$$

Note that κ_0 and κ_1 are random variables (depending on users' distances from target BS), thus we define the following statistics (expected values), which will be used later, as follows:

$$\zeta_1 \triangleq E\{\kappa_0\}, \quad \zeta_2 \triangleq E\{\kappa_0^2\}, \quad \zeta_3 \triangleq E\{\kappa_1\} \quad (37)$$

Without loss of generality, we consider BS 0 ($l = 0$) as our target BS. Thus by using the Bussgang decomposition as discussed in Sec. III, the 1-bit quantized version of (32) is

$$r_{0m}[t] = \sqrt{\gamma'} y_{0m}[t] + z_{0m}[t], \quad (38)$$

where $z_{0m}[t]$ is the QN and γ' is a scaling factor. From the previous discussion, we can show that

$$\gamma' = 2/(\pi\sigma_{y_0}^2). \quad (39)$$

Let $\mathbf{h}_{0jk} = [h_{01jk}, h_{02jk}, \dots, h_{0Mjk}]^T$ be the vector of small-scale fading gains between user k in cell j and all antennas of BS 0. Denote by $\mathbf{y}_0[t] = [y_{01}[t], \dots, y_{0M}[t]]^T$ the vector of all unquantized signals received at all antennas of BS 0 during time t , $\mathbf{r}_0[t] = [r_{01}[t], \dots, r_{0M}[t]]^T$ its corresponding quantized version and $\mathbf{z}_0[t] = [z_{01}[t], \dots, z_{0M}[t]]^T$ & $\mathbf{w}_0[t] = [w_{01}[t], \dots, w_{0M}[t]]^T$ the associated quantization and white noise vectors, respectively. We also define the $T \times 1$ vectors, $\mathbf{s}_{jk} = [s_{jk}[1], \dots, s_{jk}[T]]^T$ and $\mathbf{c}_{jk} = [c_{jk}[1], \dots, c_{jk}[T]]^T$, as the data symbols and pilot sequence of user k in the j -th cell, respectively, both over one coherence time.

Moreover, we denote by $\mathbf{D}_0 = \text{diag}[\theta_{00k}^{1/2}, \dots, \theta_{0LK}^{1/2}] \in \mathbb{R}^{KL \times KL}$ the diagonal matrix accounting for large-scale fading coefficients, $\mathbf{H}_0 = [\mathbf{h}_{001}, \dots, \mathbf{h}_{0LK}] \in \mathbb{C}^{M \times KL}$ the composite small-scale fading matrix, $\mathbf{Y}_0 = [\mathbf{y}_0[t], \dots, \mathbf{y}_0[T]] \in \mathbb{C}^{M \times T}$ the composite matrix of all received unquantized signals at all antennas during one coherence time, $\mathbf{R}_0 = [\mathbf{r}_0[t], \dots, \mathbf{r}_0[T]] \in \mathcal{A}^{M \times T}$ its quantized version, $\mathbf{C} = [\mathbf{c}_{01}, \dots, \mathbf{c}_{LK}]^T \in \mathbb{C}^{KL \times T}$ the composite pilot matrix, $\mathbf{S} = [\mathbf{s}_{01}, \dots, \mathbf{s}_{LK}]^T \in \mathbb{C}^{KL \times T}$ the composite matrix of all data symbols and $\mathbf{W}_0 = [\mathbf{w}_0[t], \dots, \mathbf{w}_0[T]]$ & $\mathbf{Z}_0 = [\mathbf{z}_0[t], \dots, \mathbf{z}_0[T]] \in \mathbb{C}^{M \times T}$ are matrices of white Gaussian noise and QN, respectively.

Then the signal impinged at all antennas of BS 0 (during one coherence time) is written in the following compact form:

$$\mathbf{Y}_0 = \sqrt{\alpha\rho}\mathbf{H}_0\mathbf{D}_0\mathbf{C} + \sqrt{\alpha\rho}\mathbf{H}_0\mathbf{D}_0\mathbf{S} + \mathbf{W}_0, \quad (40)$$

and its quantized version is

$$\mathbf{R}_0 = \sqrt{\alpha\rho\gamma'}\mathbf{H}_0\mathbf{D}_0\mathbf{C} + \sqrt{\alpha\rho\gamma'}\mathbf{H}_0\mathbf{D}_0\mathbf{S} + \sqrt{\gamma'}\mathbf{W}_0 + \mathbf{Z}_0. \quad (41)$$

B. LMMSE Channel estimate

Let $\hat{\mathbf{h}}_{00k}$ be the channel estimate of user k in the target cell. Then by the standard results on LMMSE, we can readily show that $\hat{\mathbf{h}}_{00k}$ is given by

$$\hat{\mathbf{h}}_{00k} = \xi' \mathbf{R} \mathbf{c}_{0k}^*. \quad (42)$$

where

$$\xi' \triangleq \frac{\sqrt{\alpha\rho\gamma'}}{\alpha\rho\gamma'T + \bar{\alpha}\gamma'\rho\kappa_0 + \gamma' + \sigma_z^2}. \quad (43)$$

The following lemma gives an upper bound on the average variance of estimation error.

Lemma 7. When the QN is IID, the expected value (w.r.t. large-scale fading) of $\sigma_h'^2$ is upper bounded by

$$E\{\sigma_h'^2\} = 1 - \frac{\alpha\rho T}{\alpha\rho T + (\bar{\alpha}\rho + \sigma_z^2\pi\rho/2)\zeta_1 + \sigma_z^2\pi/2 + 1}. \quad (44)$$

Proof. From the orthogonality principle of LMMSE, the variance of estimation error per single realization of k_0 is $\sigma_h'^2 = 1 - \sqrt{\alpha\rho\gamma'}\xi'$. Note that $\sigma_h'^2$ is a concave function of κ_0 . Thus, taking the expectation of $\sigma_h'^2$ w.r.t. κ_0 and making use of Jensen's inequality, (44) follows. ■

Note that, in practice, (44) serves as an approximate upper bound as there will still be some correlation between QN components. However, it turns out that the bound (44) is nearly tight in many cases as will be shown by numerical results, i.e., see Fig. 1.

C. Achievable rates analysis

We assume the BS employs MRC for data estimation as (24). Without loss of generality, we only consider the data rate for the k -th user in the 0-th cell. The output of MRC is given by

$$\hat{s}_{0k} \triangleq \frac{1}{M} \hat{\mathbf{h}}_{00k}^H \mathbf{r}_0[t] = \frac{\xi'}{M} \mathbf{c}_{0k}^T \mathbf{R}_0^H \mathbf{r}_0[t]. \quad (45)$$

Based on (45), a lower bound on the ergodic achievable rate is given in the following theorem.

Theorem 2. Consider 1-bit QSP multicell Massive MIMO with LMMSE channel estimate and MRC receiver at the BS. If power control based on statistical channel inverse is applied, then a lower bound on the achievable rate in uplink is approximated by

$$R'_{\text{QSP}} = \log(1 + \Upsilon'_{\text{QSP}}) \quad (\text{bits/s/Hz}), \quad (46)$$

where Υ'_{QSP} is given by (47), shown at the top of page 18.

Proof. See Appendix B. ■

A corollary of Theorem 2 which maximizes R'_{QSP} w.r.t. α is the following.

$$\begin{aligned} \Upsilon'_{\text{QSP}} = & \left(\alpha \bar{\alpha} \rho^2 T^2 M \right) / \left(\bar{\alpha} \rho^2 M T \zeta_3 + \frac{1}{4} (\alpha^2 \rho^2 - 8\alpha \rho^2 + 4\rho^2) \zeta_3 + \frac{1}{4} (\pi^2 \rho^2 T - \pi^2 \rho^2 - 4\alpha \rho^2 T) \zeta_2 \right. \\ & \left. + \frac{1}{4} (4\alpha \rho^2 T^2 - 2\pi^2 \rho - 4\alpha \rho T + 2\pi^2 \rho T) \zeta_1 + \frac{1}{4} (4\alpha \rho T^2 - 8\alpha^2 \rho^2 T + 8\alpha \rho^2 T + \pi^2 T - \pi^2) \right) \end{aligned} \quad (47)$$

Corollary 8. The optimal power fraction $\alpha^* \in (0, 1)$ which maximizes (46) is given by one of the two roots:

$$\alpha^* = \frac{-\delta \pm \sqrt{\delta \delta'}}{4\rho(\zeta_1 T(\rho T - 1) - \rho T(\zeta_2 + \zeta_3 M) - \zeta_3 \rho + T^2)} \quad (48)$$

where $\delta = \pi^2(T - 1)(2\zeta_1 \rho + \zeta_2 \rho^2 + 1) + 4\zeta_3 M \rho^2 T - 4\zeta_3 \rho^2$ and $\delta' = \pi^2(T - 1)(2\zeta_1 \rho + \zeta_2 \rho^2 + 1) + 4\rho T(\zeta_1 \rho T - \zeta_1 - \zeta_2 \rho + T)$.

Proof. The proof follows by following same lines of the proof of Corollary 4. ■

For the sake of comparison, we introduce the following conclusion on the achievable rate for UQSP.

Corollary 9. Under UQSP, a lowerbound on the achievable ergodic rate in uplink is

$$R'_{\text{UQSP}} = \log(1 + \Upsilon'_{\text{UQSP}}) \quad (49)$$

where Υ'_{UQSP} is defined as

$$\begin{aligned} \Upsilon'_{\text{UQSP}} = & \left(\alpha \bar{\alpha} \rho^2 T^2 M \right) / \left(\bar{\alpha} \rho^2 M T \zeta_3 + \bar{\alpha}^2 \rho^2 \zeta_3 + \bar{\alpha} \rho^2 T \zeta_2 \right. \\ & \left. + (\alpha \rho^2 T^2 + \alpha \rho T + 2\bar{\alpha} \rho T) \zeta_1 + \alpha \rho T^2 + 2\alpha \bar{\alpha} \rho^2 T + T \right) \end{aligned} \quad (50)$$

Furthermore, the optimal power fraction $\alpha^* \in (0, 1)$ which maximizes (49) is given by one of the following two roots:

$$\alpha^* = \frac{-\delta \pm \sqrt{T(\rho \zeta_1 + 1)(\rho T + 1)\delta}}{\rho T(\rho T - 1)\zeta_1 - \rho^2 T \zeta_2 - \rho(M \rho T + \rho)\zeta_3 + \rho T^2}, \quad (51)$$

where $\delta = 2\rho T \zeta_1 + \rho^2 T \zeta_2 + (\rho^2 + M \rho^2 T)\zeta_3 + T$.

Proof. Setting $\sigma_z = 0, \gamma' = 1$ and $f'(t, t) = (M + 1)\sigma_{y_0}^4 / M$ in (79) and substituting the result in (80), (49) follows. The second part follows same lines of proof as of Corollary 4. ■

D. Asymptotic results

As in the case of single-cell case, the denominators of Υ'_{QSP} and Υ'_{UQSP} are partitioned into coherent and noncoherent noises. From (47) and (50), the first term of both denominators, which is identical, corresponds to the coherent noise given by $\bar{\alpha} \rho^2 M T \zeta_3$. This implies that, for asymptotically large M , QSP and UQSP are equivalent. The following corollary is immediate.

Corollary 10. The asymptotic limit of data rates for QSP and UQSP when $M \rightarrow \infty$ is

$$R'_{\text{QSP}}{}^{M \rightarrow \infty} = R'_{\text{UQSP}}{}^{M \rightarrow \infty} = \log \left(1 + \frac{\alpha T}{\zeta_3} \right). \quad (52)$$

Note that Corollary 10 implies that QN can be averaged out as the number of BS antennas increases and hence its impact on performance can be neglected for asymptotically large M . Moreover, we have the following result:

Corollary 11. The asymptotic limits of data rates for QSP and UQSP when $\rho \rightarrow \infty$ are, respectively, given by

$$R'_{\text{QSP}}{}^{\rho \rightarrow \infty} = \log \left(1 + \Upsilon'_{\text{QSP}}{}^{\rho \rightarrow \infty} \right), \quad (53)$$

$$R'_{\text{UQSP}}{}^{\rho \rightarrow \infty} = \log \left(1 + \Upsilon'_{\text{UQSP}}{}^{\rho \rightarrow \infty} \right), \quad (54)$$

where $\Upsilon'_{\text{QSP}}{}^{\rho \rightarrow \infty}$ and $\Upsilon'_{\text{UQSP}}{}^{\rho \rightarrow \infty}$ are defined by

$$\begin{aligned} \Upsilon'_{\text{QSP}}{}^{\rho \rightarrow \infty} = & (\bar{\alpha} \alpha M T^2) / (\alpha T^2 \zeta_1 - \frac{1}{4} (4\alpha T - \pi^2 T + \pi^2) \zeta_2 \\ & \bar{\alpha} (\bar{\alpha} + M T) \zeta_3 + 2\bar{\alpha} \alpha T) \end{aligned} \quad (55a)$$

$$\Upsilon'_{\text{UQSP}}{}^{\rho \rightarrow \infty} = \frac{\alpha \bar{\alpha} M T^2}{\alpha T^2 \zeta_1 + \bar{\alpha} T \zeta_2 + \bar{\alpha} (\bar{\alpha} + M T) \zeta_3 + 2\alpha \bar{\alpha} T} \quad (55b)$$

Proof. The results unfolds from taking the limits of (46) and (49) when $\rho \rightarrow \infty$. ■

Finally, note that all rates in Corollaries 10 and 11 can be further maximized w.r.t. α as explained in the proof of Corollary 4. For instance, by inspecting Corollary 10, it is interesting to note that when $M \rightarrow \infty$, the optimal policy to maximize the data rate is to allocate all power to pilot, i.e., $\alpha \rightarrow 1$.

VI. NUMERICAL RESULTS

In this section, we present some numerical results to compare the analytical bounds in Theorem 2 and Corollaries 9- 11 for QSP and UQSP with the results obtained by Monte Carlo (MC) simulation. Furthermore, we include the simulation result for QTP, where we assume $\tau = K$ and no optimization over power or training length is performed, i.e., non-optimized QTP. Also, we assume random pilot assignment for QTP, where each user is assigned a pilot sequence randomly from a fixed set of pilot sequences and the pilot sequences of each K users in any cell are mutually orthogonal. In all MC simulations, the rates are maximized (w.r.t. α) per single realization of large-scale fading and thus the final rate is taken to be the average over many such realizations. Moreover, we include the simulation results when PR is implemented after estimating the channel. This will allow us to see the gap with our analytical results. We assume the BS removes pilot contribution of its users only.

In our model, we consider a hexagonal network of one tier of BSs, i.e., $L = 7$. Each cell has a radius $r_c = 1.8$ Km with a forbidden region of radius $r_f = 0.1$ Km in which no user is allowed to exist. The channel is assumed Rayleigh block-fading with bandwidth $B_w = 200$ KHz and each block is transmitted within 1 ms (coherence time of channel in seconds, i.e., one subframe in LTE). This is translated into a coherence time $T = 200$ (in symbol intervals). All users are distributed uniformly and randomly within each

cell. The large-scale fading coefficient β_{0jk} is defined by $\beta_{0jk} = \omega^{-1} d_{0jk}^{-\zeta}$ [21] [18], where d_{0jk} is the distance (in Km) from the k -th user in cell j to BS 0, $\zeta = 3.8$ is the path-loss exponent and ω is the path-loss at a reference distance of 1 Km, which also accounts for distance-independent propagation losses such as wall penetration. The statistics ζ_1, ζ_2 and ζ_3 defined in (37) which are needed for computing the analytical results are obtained by MC simulation, where they converge to fixed values depending on the geometry of the network, such as the radii of cell and forbidden region. According to our cell settings, we observe that including more tiers (say, second tier or $L = 19$) changes the computed statistics slightly. For convenience, the system parameters are summarized in Table I.

TABLE I
SIMULATION PARAMETERS

Parameter	Value / Description
Cell layout	One-tier hexagonal, $L = 7$
System bandwidth (B_w)	200 KHz
Coherence time (T)	200 symbol intervals (1ms)
Cell radius (r_c)	1.8Km
Forbidden region radius (r_f)	0.1Km
Path-loss exponent (ζ)	3.8
$\zeta_1 = E\{k_0\}$	$\approx 1.4116K$
$\zeta_3 = E\{k_1\}$	$\approx 1.1656K$
$\zeta_2 = E\{k_0^2\}$	$\approx 50.53, 288.6, 450.66, 1248.94$ when $K = 5, 12, 15, 25$

TABLE II
THE OPTIMAL POWER FRACTION α^* FOR DIFFERENT M ,
 $K = 12, T = 200, \text{SNR} = -10\text{dB}$. ALL SIMULATION RESULTS ARE
AVERAGED OVER LARGE-SCALE FADING.

No. of BS antennas M	50	200	600	1000
MC QSP	0.34	0.41	0.50	0.59
MC QSP PR	0.38	0.43	0.53	0.59
Anal. QSP (48)	0.38	0.45	0.55	0.61
MC UQSP	0.33	0.44	0.57	0.65
MC UQSP PR	0.40	0.49	0.6	0.64
Anal. UQSP (51)	0.33	0.44	0.56	0.62

In Fig. 1 the average variance of channel estimation error (i.e., averaged over large-scale fading) is compared with the approximate upper-bound in Lemma 7. It is obvious that there is a close match between the empirical and analytical analysis, especially when SNR is low. Undoubtedly, the approximate upper bound in Lemma 7 serves as a very good approximation of variance of channel estimation error for all SNR values. Moreover, the performance improves as T increases which is an intuitive result.

Figure 2 illustrates the average SNR versus the achievable rates for the QSP, UQSP and QTP. For QSP, it is clear that the analytical bound (46) works as a good approximation for the rate under QSP, especially when PR is used. It is obvious that the analytical approximation is more accurate in the very low SNR regime and overestimates the achievable rate slightly in other SNR regions. The latter should come at no surprise due to the approximation made in deriving (46), where some terms that contribute to the increase of effective noise have been neglected, primarily, due to the IID assumption on QN

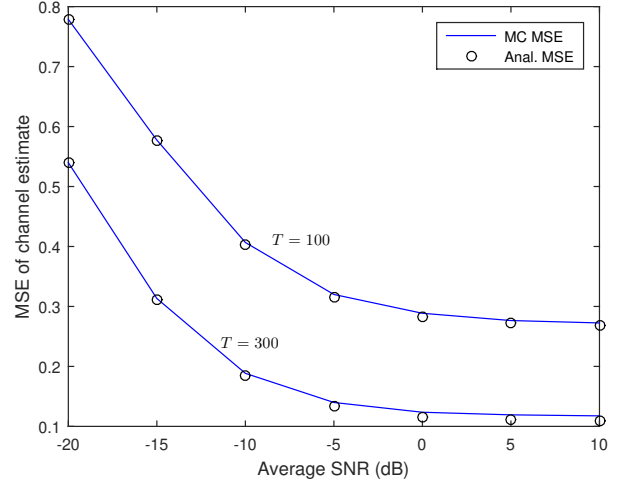


Fig. 1. Average SNR vs. MSE of channel estimate for a fixed power allocation in QSP, $L = 7, K = 12, M = 100, \alpha = 0.5$.

(see Appendices B and A). For UQSP, the analytical lower bound (49) and MC result with no PR are almost the same¹. Also, it can be seen that QSP outperforms the non-optimized QTP.

We observe that all rates for QSP, UQSP and QTP converge to fixed values as SNR grows large as shown in Fig. 2, where we also show the analytical asymptotes obtained from Corollary 11 for QSP and UQSP. With a moderate $M = 100$, we observe that the gap between QSP & UQSP with PR and QSP & UQSP with no PR is almost the same; ranges from 0.144bps/Hz at -20dB (very low SNR) to 0.52bps/Hz at 10dB (high SNR), implying that under a multicell scenario with 1-bit ADCs, the loss in information is not significant compared with infinite-resolution ADCs. Thus it is expected that when the number of quantization bits increases (say, 2 or 3 bits), this gap becomes less pronounced.

In Fig. 3 we demonstrate the impact of increasing the number of users K on the performance for QSP². Note that as K increases, the per-user data rate decreases, which is a natural consequence of the increases of interference (in our case, data interference from all users). As expected, we observe that when K increases, our analytical approximation for QSP becomes more accurate. This is because the IID assumption on QN becomes more accurate as K increases as mentioned under Assumption 3. We also observe that at very low SNR (-20dB), a close match between analytical and simulation results, owing to the fact that when SNR is low, QN becomes approximately IID, rendering our analytical approximation more accurate (see also Assumption 3). In Massive MIMO, highly-loaded networks with tens of users are served simultaneously by each BS is expected [8], thereby making our analytical bound (46) a very good approximation of the performance. Finally, we observe that in almost all cases, QSP

¹Note that when deriving (49), no approximations have been made as those made under QSP. Thus any gap between the simulation and analytical results is due to Jensen's inequality, see the proof of Corollary 9.

²Note that K enters the effective SNR equation (47) through the statistics ζ_1, ζ_2 and ζ_3 .

Fig. 2. The achievable rate vs. SNR for QSP and UQSP, $L = 7, K = 12, M = 100, T = 200$.

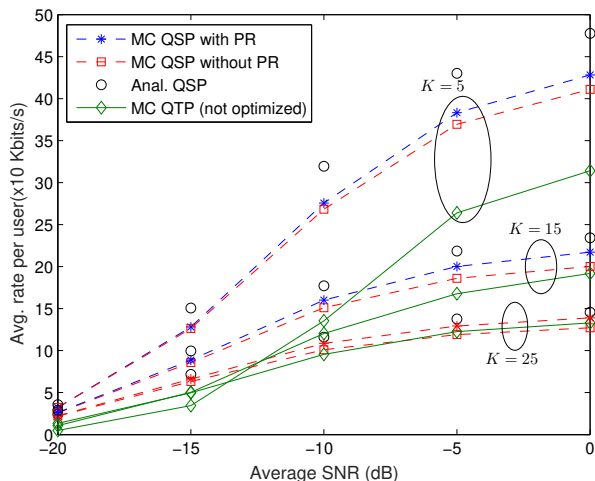


Fig. 3. The impact of number of users K on the achievable rate for QSP, $L = 7, M = 100, T = 200$.

outperforms QTP. However, the gap in performance becomes less pronounced as K increases.

Figure 4 depicts the impact of increasing BS antennas M on performance. Associated with Fig. 4, Table II shows the average power fraction α computed by MC simulation for QSP and UQSP when $M = 50, 200, 600, 1000$. Note that for all cases, the common trend for the optimal value of α is that it increases as M increases. This is consistent with Corollary 10, where the optimal policy to maximize the data rate when $M \rightarrow \infty$ is to allocate most power to pilot. From Fig. 4, we can see that, for all cases, increasing M gives rise to an increase in data rates. Also we observe that QSP outperforms QTP as was observed previously.

Obviously, the data rate achieved when using PR is higher than when no PR is employed. However, the gap is not significant, especially under the quantized system. It can also be observed that the analytical approximation for QSP serves

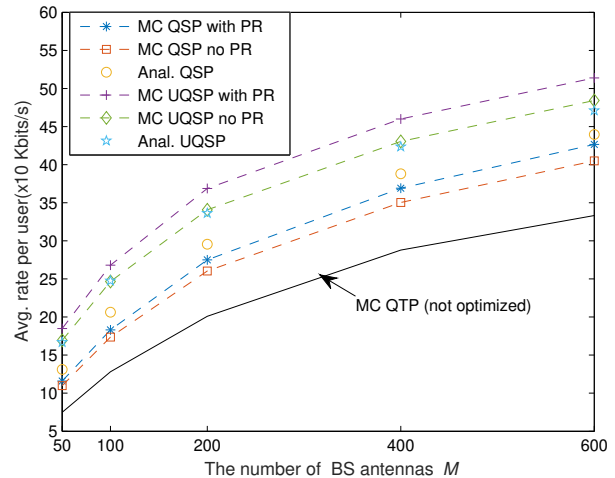


Fig. 4. The achievable rate vs. no. of BS antennas M , $L = 7, K = 12, T = 200$ and SNR = -10 dB.

as a good approximation for the data rate, particularly, when PR is employed. The interpretation for this is as follows. In our analytical analysis, many terms contributing small quantities to the noise variance have been neglected, thus the noise variance is underestimated. i.e., see Appendices B & C for more details. However, when PR is employed, the variance of noise is further reduced due to the subtraction of pilot interference from the MRC output, thus, this reduction of noise variance, in some sense, compensates for the underestimation made in the analytical bound. This is clear from the closeness between the analytical approximation and simulated QSP with PR. Clearly, more antennas are needed under QSP to achieve same data rate as under UQSP. For small or medium number of BS antennas, we observe that the ratio between number of antennas for QSP to the number of antennas for UQSP is roughly 2, however, this ratio decreases gradually as M increases due to the asymptotic convergence of data rates for both schemes, as will be seen next.

Figure 5 demonstrates the asymptotic behaviour when M grows unboundedly. The analytical asymptote in Corollary 10 is also shown for comparison. Observe that for all cases, the data rate increases gradually as M increases and finally converges to fixed values. This implies that, for asymptotically large M , quantization incurs no loss of information, when compared with the infinite-resolution counterpart.

Finally, we would like to emphasize, nevertheless, that QSP can outperform QTP in most simulated cases, a fair comparison between QSP and QTP requires to take into account pilot contamination in SP scheme (i.e., when $T < KL$), the use of more advanced signal processing techniques other than MRC and optimization over training length/power for QTP. This needs more investigations and hence left for future work.

VII. CONCLUSION

In this paper, we obtained closed-form expressions for the uplink data rates in 1-bit QSP Massive MIMO in single-cell and multicell cases. For comparison with the “no quantization”

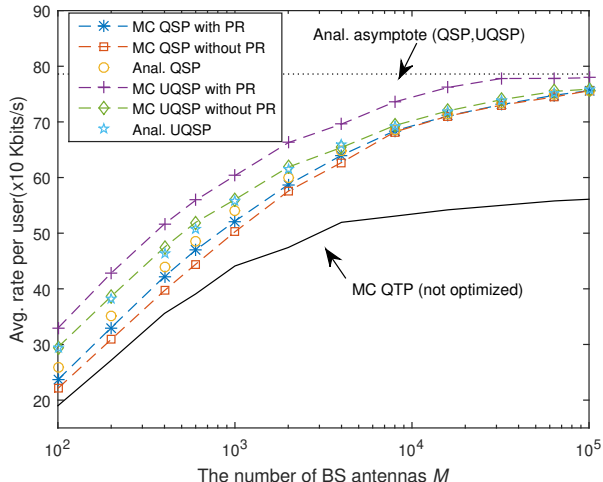


Fig. 5. The asymptotic behaviour of data rate w.r.t. the number of BS antennas, $L = 7$, $K = 12$, $T = 200$, $\text{SNR} = -5\text{dB}$.

case, we leveraged the results obtained for QSP to derive a lower bound on achievable rate for UQSP. We have shown that quantization noise doesn't scale with the number of BS antennas and hence can be averaged out as M grows large. We have demonstrated that, regardless the coarse quantization and pilot-data superposition, high data rates can be achieved in practical multicell scenarios. Interestingly, for asymptotically large M , the rates achieved under QSP and UQSP saturate and converge to the same deterministic value. We have also shown the performance of the non-optimized QTP, where the length of training τ is assumed the same as the number of users K . In most simulated cases, it is shown that QSP outperforms QTP.

APPENDIX

A. Proof of Theorem 1

In this subsection, we prove Theorem 1. To that end, we need the following lemmas.

Lemma 12.

$$\mathbb{E} \left\{ \|\mathbf{y}[t]\|^2 \right\} = M\sigma_y^2, \quad (56a)$$

$$\mathbb{E} \left\{ \|\mathbf{y}[t]\|^4 \right\} = M(M+1)\sigma_y^4, \quad (56b)$$

Proof. The above results follow straightforwardly since the entries of $\mathbf{y}[t]$ are assumed IID $\mathcal{CN}(0, \sigma_y^2)$. ■

Lemma 13. For any two time instants n and q , we have

$$\lim_{M \rightarrow \infty} \frac{\mathbf{z}^H[n]\mathbf{y}[q]}{M} = \mathbb{E} \{ z_1^*[n]y_1[q] \} = 0, \forall n, q \quad (57a)$$

$$\lim_{M \rightarrow \infty} \frac{\mathbf{z}[n]^H\mathbf{z}[q]}{M} = \begin{cases} \mathbb{E} \{ z_1^*[n]z_1[q] \} = 0, n \neq q \\ \mathbb{E} \{ |z_1[n]|^2 \} = \sigma_z^2, n = q \end{cases} \quad (57b)$$

Proof. The above results unfolds from the fact that each column of \mathbf{Y} and \mathbf{Z} consist of IID entries and hence each inner product consists of a sum of M IID entries with same mean and variance. By the LLN, as $M \rightarrow \infty$, the right-hand

sides (RHSs) of (57a) and (57b) follow from (9) and (12), respectively. ■

Lemma 14. For any $n \neq q$, with Assumption 3 holds, the following conditional densities satisfy (approximately)

$$p(\mathbf{z}[n]|\mathbf{z}[q]) = p(\mathbf{z}[n]) \quad (58)$$

$$p(z[n]|y[q]) = p(z[n]). \quad (59)$$

Proof. Equation (58) follows because the QN is IID. Since QN is a function of the unquantized signal and the IID assumption on QN implies that QN at time n is a function of the unquantized signal received at time n only and independent of any signal received at other time instants, hence (59) follows. ■

Lemma 15. For any $n \neq q$ we have

$$\mathbb{E} \{ \mathbf{y}[n]|\mathbf{y}[q] \} = \frac{\alpha \rho \bar{\mathbf{c}}^H[q] \bar{\mathbf{c}}[n]}{\sigma_y^2} \mathbf{y}[q] \quad (60)$$

Proof. The proof follows from applying standard MMSE or equivalently LMMSE since both vectors are assumed Gaussian, i.e., MMSE estimate of $\mathbf{y}[n]$ given the observation $\mathbf{y}[q]$. ■

Now, by decomposing the output of MRC (24) into two parts; signal and uncorrelated effective noise, (24) can be rewritten as

$$\hat{s}_k[t] = a_k s_k[t] + \epsilon_k[t], \quad (61)$$

where a_k is a deterministic constant and $\epsilon_k[t]$ is the effective non-Gaussian noise which is uncorrelated with $s_k[t]$ or equivalently, the noise has smallest variance. From orthogonality principle, we have

$$a_k = \mathbb{E} \{ s_k^*[t] \hat{s}_k[t] \}. \quad (62)$$

and hence the variance of noise $\epsilon_k[t]$ is given by $\sigma_{\epsilon_k}^2 = \mathbb{E} \{ |\hat{s}_k[t]|^2 \} - |\mathbb{E} \{ \hat{s}_k[t] \}|^2 - |a_k[t]|^2$.

For the sake of comparison with UQSP approach, we define

$$\tilde{\sigma}_{\epsilon_k}^2 = \sigma_{\epsilon_k}^2 / |a_k[t]|^2. \quad (63)$$

as the variance of *normalized effective noise*. Since $s_k[t]$ is Gaussian, a lower bound on channel capacity is obtained by replacing $\epsilon_k[t]$ by a Gaussian noise with same variance $\sigma_{\epsilon_k}^2$. Thus the lower bound is

$$R^{\text{LB}} = \log(1 + 1/\tilde{\sigma}_{\epsilon_k}^2). \quad (64)$$

1) Calculation of a_k : Expanding (24) yields

$$\hat{s}_k[t] = \frac{\xi}{M} \sum_{n=1}^T c_k[n] \left(\gamma \mathbf{y}^H[n] \mathbf{y}[t] + \mathbf{z}^H[n] \mathbf{z}[t] \right) + \sqrt{\gamma} \mathbf{y}^H[n] \mathbf{z}[t] + \sqrt{\gamma} \mathbf{z}^H[n] \mathbf{y}[t]. \quad (65)$$

Using (65) in (62) gives

$$\begin{aligned} a_k &\approx \frac{\xi}{M} \sum_{n=1}^T c_k[n] \gamma \mathbb{E} \{ \mathbf{y}^H[n] \mathbf{y}[t] s_k^*[t] \} \\ &= \sqrt{\bar{\alpha}} \alpha \rho \gamma \xi T, \end{aligned} \quad (66)$$

where the approximation in the first line follows from using Lemma 13.

2) Calculation of $\tilde{\sigma}_{\epsilon_k}^2$: Using (65), we can verify that

$$\begin{aligned} \mathbb{E}\{\hat{s}_k[t]\} &= \xi(\alpha\rho\gamma T + \bar{\alpha}\rho\gamma K + \gamma + \sigma_z^2)c_k[t] \\ &= \sqrt{\alpha\rho\gamma}c_k[t] \end{aligned} \quad (67)$$

where in (67) we have made use of Lemma 1 and the assumption that quantization noise samples are i.i.d. each with zero-mean and variance σ_z^2 , i.e., see Assumption 3 and (12). From (24), $\mathbb{E}\{|\hat{s}_k[t]|^2\}$ can be written as

$$\begin{aligned} \mathbb{E}\{|\hat{s}_k[t]|^2\} &= \frac{\xi^2}{M^2} \mathbf{c}_k^T \mathbb{E}\{\mathbf{R}^H \mathbf{r}[t] \mathbf{r}[t]^H \mathbf{R}\} \mathbf{c}_k^* \\ &= \xi^2 f(t, t) + \xi^2 \sum_{\substack{n, q=1 \\ (n, q) \neq (t, t)}}^T c_k[n] c_k^*[q] f(n, q) \end{aligned} \quad (68)$$

where $f(n, q) \triangleq \mathbb{E}\{\mathbf{r}[n]^H \mathbf{r}[t] \mathbf{r}[t]^H \mathbf{r}[q]\} / M^2$. Using the definition of quantized signal, we can express $f(n, q)$ in terms of unquantized signal and quantization noise as follows:

$$\begin{aligned} f(n, q) &= \frac{1}{M^2} \left(f_1 + f_2 + 2\Re\{f_3\} + f_4 + f_5 + 2\Re\{f_6\} \right. \\ &\quad \left. + 2\Re\{f_7\} + 2\Re\{f_8\} + 2\Re\{f_9\} + 2\Re\{f_{10}\} \right) \end{aligned} \quad (69)$$

where the terms $f_1 - f_{10}$ are given by

$$f_1 = \gamma^2 \mathbb{E}\{\mathbf{y}^H[n] \mathbf{y}[t] \mathbf{y}^H[t] \mathbf{y}[q]\} \quad (70a)$$

$$f_2 = \mathbb{E}\{\mathbf{z}^H[n] \mathbf{z}[t] \mathbf{z}^H[t] \mathbf{z}[q]\} \quad (70b)$$

$$f_3 = \gamma \mathbb{E}\{\mathbf{y}^H[n] \mathbf{y}[t] \mathbf{z}^H[t] \mathbf{z}[q]\} \quad (70c)$$

$$f_4 = \gamma \mathbb{E}\{\mathbf{y}^H[n] \mathbf{z}[t] \mathbf{z}^H[t] \mathbf{y}[q]\} \quad (70d)$$

$$f_5 = \gamma \mathbb{E}\{\mathbf{z}^H[n] \mathbf{y}[t] \mathbf{y}^H[t] \mathbf{z}[q]\} \quad (70e)$$

$$f_6 = \gamma^{\frac{3}{2}} \mathbb{E}\{\mathbf{y}^H[n] \mathbf{z}[t] \mathbf{y}^H[t] \mathbf{y}[q]\} \quad (70f)$$

$$f_7 = \gamma^{\frac{3}{2}} \mathbb{E}\{\mathbf{y}^H[n] \mathbf{y}[t] \mathbf{y}^H[t] \mathbf{z}[q]\} \quad (70g)$$

$$f_8 = \gamma \mathbb{E}\{\mathbf{y}^H[n] \mathbf{z}[t] \mathbf{y}^H[t] \mathbf{z}[q]\} \quad (70h)$$

$$f_9 = \gamma^{\frac{1}{2}} \mathbb{E}\{\mathbf{y}^H[n] \mathbf{z}[t] \mathbf{z}^H[t] \mathbf{z}[q]\} \quad (70i)$$

$$f_{10} = \gamma^{\frac{1}{2}} \mathbb{E}\{\mathbf{z}^H[n] \mathbf{y}[t] \mathbf{z}^H[t] \mathbf{z}[q]\}. \quad (70j)$$

It is clear that the evaluation of $f_2 - f_{10}$ when $(n, q) \neq (t, t)$ is challenging since $\mathbf{r}[n], \mathbf{r}[t]$ and $\mathbf{r}[q]$ are not independent, in general. Therefore, in the following we shall make use of Assumption 3 in Sec. III-A alongside the asymptotic analysis to obtain a closed-form yet a good approximation for $\tilde{\sigma}_{\epsilon_k}^2$. Making use of Lemmas 12- 15, we can show that

$$\frac{f_2}{M} \approx \begin{cases} \sigma_z^4, & n = q \neq t, \\ 0, & \text{else} \end{cases} \quad (71)$$

$$\frac{f_3}{M^2} \approx \begin{cases} \alpha\rho\gamma\sigma_z^2 \bar{\mathbf{c}}^H[t] \bar{\mathbf{c}}[n], & q = t, n \neq t \\ 0, & \text{else} \end{cases} \quad (72)$$

$$\frac{f_4}{M} = \frac{f_5}{M} \approx \begin{cases} \gamma\sigma_z^2\sigma_y^2, & n = q \neq t \\ 0, & \text{else} \end{cases} \quad (73)$$

$$f_6 = f_7 = \dots = f_{10} \approx 0. \quad (74)$$

Combining (70a), (74)- (71), (69) and (68) gives

$$\begin{aligned} \mathbb{E}\{|\hat{s}_k[t]|^2\} &\approx \frac{\xi^2}{M^2} f(t, t) + \frac{\xi^2 \gamma^2}{M^2} \mu_1 + 2\alpha\rho\xi^2\sigma_z^2\gamma(T - K) \\ &\quad + \frac{\xi^2\sigma_z^4}{M}(T - 1) + \frac{2\xi^2\gamma\sigma_z^2\sigma_y^2}{M}(T - 1) \end{aligned} \quad (75)$$

where $\mu_1 = \mathbb{E}\{\mathbf{c}_k^T \mathbf{Y}^H \mathbf{y}[t] \mathbf{y}^H[t] \mathbf{Y} \mathbf{c}_k^*\} - M(M+1)\sigma_y^4$. In (75), the second term is due to f_1 , third to f_3 , fourth to f_2 and fifth to f_4 & f_5 . After some mathematical manipulations, we can verify that:

$$\begin{aligned} \mu_1 &= \alpha^2 \rho^2 M T^2 (K + M) + \bar{\alpha}^2 \rho^2 K M (K M + K T + M T + 1) \\ &\quad + \bar{\alpha} \alpha \rho^2 K M T (K + M) + 2 \bar{\alpha} \rho K M^2 \\ &\quad + \bar{\alpha} \alpha \rho^2 M T^2 (K + M) + 2 \bar{\alpha} \alpha \rho^2 M T (K M + 1) \\ &\quad + 2 \bar{\alpha} \rho K M T + \alpha \rho K M T + 2 \alpha \rho M^2 T + \alpha \rho M T^2 \\ &\quad + M(M + T) - M(M + 1)(K \rho + 1)^2. \end{aligned} \quad (77)$$

Substituting (77) in (75) and combining the result with (67), (62) and (63) yields the closed-form expression for $\tilde{\sigma}_{\epsilon_k}^2$ given in (76), which is shown at the top of page 29. Finally, substituting (76) with $f(t, t) = 1$ in (64) yields (25). This completes the proof.

B. Proof of Theorem 2

We begin by using the decomposition in (61). Redefining $a_k, s_k[t]$ and $\epsilon_k[t]$ as $a_{0k}, s_{0k}[t]$ and $\epsilon_{0k}[t]$, respectively, (45) can be written as $\hat{s}_{0k} = a_{0k} s_{0k}[t] + \epsilon_{0k}[t]$. Let

$$\tilde{\sigma}_{\epsilon_{0k}}^2 = (\mathbb{E}\{|\hat{s}_{0k}[t]|^2\} - |\mathbb{E}\{\hat{s}_{0k}[t]\}|^2) / |a_{0k}|^2 - 1, \quad (78)$$

be the normalized variance of effective noise at the output of MRC and hence the lower bound on achievable rate is

$$R^{\text{LB}} = \mathbb{E}\{\log(1 + 1/\tilde{\sigma}_{\epsilon_{0k}}^2)\} \geq \log(1 + 1/\mathbb{E}\{\tilde{\sigma}_{\epsilon_{0k}}^2\}), \quad (80)$$

where the expectation is taken w.r.t. large-scale fading and the inequality follows from applying Jensen's inequality.

Thus our task is to calculate (78). Following the same lines of proof in Appendix A, it is easy to show that a_{0k} and $\mathbb{E}\{\hat{s}_{0k}[t]\}$ are given by:

$$a_{0k} \approx \xi' \gamma' \rho T \sqrt{\bar{\alpha} \alpha} \quad (81a)$$

$$\mathbb{E}\{\hat{s}_{0k}[t]\} = \sqrt{\alpha \rho \gamma'} c_{0k}[t], \quad (81b)$$

where the approximation sign in (81a) is due to Lemma 13.

Using (68) and after redefining all parameters according to the signal model (41), $\mathbb{E}\{|\hat{s}_{0k}[t]|^2\}$ can be written as

$$\begin{aligned} \mathbb{E}\{|\hat{s}_{0k}[t]|^2\} &= \xi'^2 f'(t, t) \\ &\quad + \xi'^2 \sum_{\substack{n, q=1 \\ (n, q) \neq (t, t)}}^T c_{0k}[n] c_{0k}^*[q] f'(n, q), \end{aligned} \quad (82)$$

where $f'(n, q) \triangleq \mathbb{E}\{\mathbf{r}_0[n]^H \mathbf{r}_0[t] \mathbf{r}_0[t]^H \mathbf{r}_0[q]\} / M^2$, and ξ' is given in (43). Expanding $f'(n, q)$ as (69) we get

$$\begin{aligned} f'(n, q) &= \frac{1}{M^2} \left(f'_1 + f'_2 + 2\Re\{f'_3\} + f'_4 + f'_5 + 2\Re\{f'_6\} \right. \\ &\quad \left. + 2\Re\{f'_7\} + 2\Re\{f'_8\} + 2\Re\{f'_9\} + 2\Re\{f'_{10}\} \right) \end{aligned} \quad (83)$$

$$\begin{aligned} \tilde{\sigma}_{\epsilon_k}^2 = & \left(M^2 f(t, t) - \gamma^2 M \left(\rho^2 (K^2 (M - \bar{\alpha}T + 1) - K (\bar{\alpha}MT + \alpha (\alpha + T^2 - 2) + 1) - 2\bar{\alpha}\alpha T) + \rho(2K(M - T + 1) \right. \right. \\ & \left. \left. + \alpha T(K - T)) + M - T + 1 \right) + M(T - M - 1) (2\gamma(K\rho + 1) + \sigma_z^2) \sigma_z^2 \right) / \left(\alpha\bar{\alpha}\rho^2\gamma^2 M^2 T^2 \right) \end{aligned} \quad (76)$$

$$\begin{aligned} \tilde{\sigma}_{\epsilon_{0k}}^2 = & \left(M^2 f'(t, t) + \gamma'^2 M \rho (\kappa_0 (\kappa_0 \rho (\bar{\alpha}T - M - 1) - 2M + T(\alpha + 2\bar{\alpha} + \alpha\rho T) - 2) + \bar{\alpha}\rho(\bar{\alpha} + MT)\kappa_1) \right. \\ & \left. + \gamma'^2 M(-M + T(\alpha\rho(2\bar{\alpha}\rho + T) + 1) - 1) + M(T - M - 1) (2\gamma'(\kappa_0\rho + 1) + \sigma_z^2) \sigma_z^2 \right) / \left(\alpha\bar{\alpha}\gamma'^2 M^2 \rho^2 T^2 \right) \end{aligned} \quad (79)$$

where we redefine $\{f_j\}$ as $\{f'_j\}$ with replacing all quantized signal and QN vectors in (70a)- (70j) according to (41). Following the same lines of proof as previously, (82) can be readily written as

$$\begin{aligned} E\{|\hat{s}_{0k}[t]|^2\} \approx & \xi'^2 f'(t, t) + \frac{\xi'^2 \gamma'^2}{M^2} \mu'_1 + 2\alpha\rho\xi'^2 \sigma_z^2 \gamma'(T - \kappa_0) \\ & + \frac{\xi'^2 \sigma_z^4}{M} (T - 1) + \frac{2\xi'^2 \gamma' \sigma_z^2 (\kappa_0 \rho + 1)^2}{M} (T - 1), \end{aligned} \quad (84)$$

where μ'_1 is given by

$$\begin{aligned} \mu'_1 = & E\{\mathbf{c}_{0k}^T \mathbf{Y}_0^H \mathbf{y}_0[t] \mathbf{y}_0^H[t] \mathbf{Y}_0 \mathbf{c}_{0k}^*\} - M(M + 1)\sigma_{y_0}^4 \\ = & M \left(\left(2\alpha M \rho^2 T - 2\alpha M \rho - 2\alpha^2 M \rho^2 T - 2\rho + \alpha\rho^2 T^2 \right. \right. \\ & \left. \left. - \alpha\rho T + 2\rho T \right) \kappa_0 + \left(\alpha^2 M \rho^2 - 2\alpha M \rho^2 - \rho^2 - \alpha\rho^2 T \right. \right. \\ & \left. \left. + \rho^2 T \right) \kappa_0^2 + \bar{\alpha}\rho^2 (MT + \bar{\alpha})\kappa_1 + \alpha M \rho^2 T^2 + 2\alpha M \rho T \right. \\ & \left. + \alpha\rho T^2 - 2\alpha^2 \rho^2 T + 2\alpha\rho^2 T + T - 1 \right). \end{aligned} \quad (85)$$

Combining (85), (84), (81) and (78), and after some mathematical manipulations and plugging all related equations in (78), we obtain (79), which is shown on the top of page 30. Substituting (39), (43), and $f'(t, t) = 1$ in (79), we obtain $\tilde{\sigma}_{\epsilon_{0k}}^2$, i.e., per single realization of large-scale fading. Finally, the lower bound (46) follows from (80). This completes the proof.

REFERENCES

- [1] B. Murmann, "A/D converter trends: Power dissipation, scaling and digitally assisted architectures," in *2008 IEEE Custom Integrated Circuits Conference*, Sept 2008, pp. 105–112.
- [2] R. H. Walden, "Analog-to-digital converter survey and analysis," *IEEE Journal on Selected Areas in Communications*, vol. 17, no. 4, pp. 539–550, Apr 1999.
- [3] C. Risi, D. Persson, and E. G. Larsson, "Massive MIMO with 1-bit ADC," *CoRR*, vol. abs/1404.7736, 2014. [Online]. Available: <http://arxiv.org/abs/1404.7736>
- [4] S. Jacobsson, G. Durisi, M. Coldrey, U. Gustavsson, and C. Studer, "Throughput analysis of massive MIMO uplink with low-resolution ADCs," *IEEE Transactions on Wireless Communications*, vol. 16, no. 6, pp. 4038–4051, June 2017.
- [5] C. Studer and G. Durisi, "Quantized massive MU-MIMO-OFDM uplink," *IEEE Transactions on Communications*, vol. 64, no. 6, pp. 2387–2399, June 2016.
- [6] S. Hoyos, B. M. Sadler, and G. R. Arce, "Monobit digital receivers for ultrawideband communications," *IEEE Transactions on Wireless Communications*, vol. 4, no. 4, pp. 1337–1344, July 2005.
- [7] M. T. Ivrlač and J. A. Nossek.
- [8] T. L. Marzetta, "Noncooperative cellular wireless with unlimited numbers of base station antennas," *IEEE Transactions on Wireless Communications*, vol. 9, no. 11, pp. 3590–3600, November 2010.
- [9] C. Mollen, J. Choi, E. G. Larsson, and R. W. Heath, "Uplink performance of wideband massive MIMO with one-bit ADCs," *IEEE Transactions on Wireless Communications*, vol. 16, no. 1, pp. 87–100, Jan 2017.
- [10] Y. Li, C. Tao, G. Seco-Granados, A. Mezghani, A. L. Swindlehurst, and L. Liu, "Channel estimation and performance analysis of one-bit massive MIMO systems," *IEEE Transactions on Signal Processing*, vol. 65, no. 15, pp. 4075–4089, Aug 2017.
- [11] J. Bussgang, "Crosscorrelation functions of amplitude-distorted gaussian signals," *RLE Technical Reports*, vol. 216, 1952.
- [12] B. Hassibi and B. M. Hochwald, "How much training is needed in multiple-antenna wireless links?" *IEEE Transactions on Information Theory*, vol. 49, no. 4, pp. 951–963, April 2003.
- [13] T. Marzetta, "How much training is required for multiuser MIMO?" in *40th Asilomar Conf. on Signals, Systems, & Computers*, Pacific Grove, CA, Oct. 2006, pp. 359–363.
- [14] G. Zhou, M. Viberg, and T. McKelvey, "Superimposed periodic pilots for blind channel estimation," in *Signals, Systems and Computers, 2001. Conference Record of the Thirty-Fifth Asilomar Conference on*, vol. 1, Nov 2001, pp. 653–657 vol.1.
- [15] J. Tugnait and W. Luo, "On channel estimation using superimposed training and first-order statistics," *Communications Letters, IEEE*, vol. 7, no. 9, pp. 413–415, Sept 2003.
- [16] J. Wang and X. Wang, "Superimposed training-based noncoherent MIMO systems," *Communications, IEEE Transactions on*, vol. 54, no. 7, pp. 1267–1276, July 2006.
- [17] K. Upadhyay, S. A. Vorobyov, and M. Vehkaperä, "Superimposed pilots are superior for mitigating pilot contamination in massive MIMO," *IEEE Transactions on Signal Processing*, vol. 65, no. 11, pp. 2917–2932, June 2017.
- [18] D. Verenzuela, E. Björnson, and L. Sanguinetti, "Spectral and Energy Efficiency of Superimposed Pilots in Uplink Massive MIMO," *ArXiv e-prints*, Sep. 2017.
- [19] A. Mezghani and J. a. Nossek, "Capacity Lower Bound of MIMO Channels with Output Quantization and Correlated Noise," *IEEE International Symposium on Information Theory*, no. 3, pp. 1732–1736, 2012.
- [20] G. Jacovitti and A. Neri, "Estimation of the autocorrelation function of complex Gaussian stationary processes by amplitude clipped signals," *IEEE Transactions on Information Theory*, vol. 40, no. 1, pp. 239–245, Jan 1994.
- [21] E. Björnson, L. Sanguinetti, and M. Kountouris, "Deploying dense networks for maximal energy efficiency: Small cells meet massive MIMO," *IEEE Journal on Selected Areas in Communications*, vol. 34, no. 4, pp. 832–847, April 2016.

